

MirrorLA: Reflecting Feature Map for Vision Linear Attention

Weikang Meng^{1,2} Liangyu Huo¹ Yadan Luo³ Yaowei Wang^{1,2} Yingjian Li² Zheng Zhang^{1,†}

¹Harbin Institute of Technology, Shenzhen ²Pengcheng Laboratory ³UQMM Lab, University of Queensland

†Corresponding author

Abstract

Linear attention significantly reduces the computational complexity of Transformers from quadratic to linear, yet it consistently lags behind softmax-based attention in performance. We identify the root cause of this degradation as the non-negativity constraint imposed on kernel feature maps: standard projections like ReLU act as “passive truncation” operators, indiscriminately discarding semantic information residing in the negative domain. We propose MirrorLA, a geometric framework that substitutes passive truncation with active reorientation. By leveraging learnable Householder reflections, MirrorLA rotates the feature geometry into the non-negative orthant to maximize information retention. Our approach restores representational density through a cohesive, multi-scale design: it first optimizes local discriminability via block-wise isometries, stabilizes long-context dynamics using variance-aware modulation to diversify activations, and finally, integrates dispersed subspaces via cross-head reflections to induce global covariance mixing. MirrorLA achieves state-of-the-art performance across standard benchmarks, demonstrating that strictly linear efficiency can be achieved without compromising representational fidelity.

Correspondence: darrenzz219@gmail.com

1 Introduction

Transformer-based models (Vaswani et al., 2017; Dosovitskiy et al., 2021) have become the dominant paradigm for modeling long-range dependencies in vision and language tasks. Their success largely stems from the self-attention mechanism, which aggregates global context via softmax-normalized dot-product similarity. Despite its effectiveness, softmax attention suffers from a quadratic computational complexity $O(N^2d)$ relative to the sequence length N , making it prohibitively expensive for long sequences and high-resolution visual inputs.

Linear Attention (LA) (Katharopoulos et al., 2020; MiniMax et al., 2025; Meng et al., 2025) addresses this limitation by reformulating softmax attention using kernel feature maps that enable associative reordering of matrix multiplications. This reformulation shifts the computation order from $\text{Softmax}(\mathbf{Q}\mathbf{K}^\top)\mathbf{V}$ to $\phi(\mathbf{Q})(\phi(\mathbf{K})^\top\mathbf{V})$. Consequently, the complexity is reduced to $O(Nd^2)$, maintaining the benefits of global context modeling while ensuring computational efficiency for resource-intensive tasks. However, despite extensive research, linear attention methods consistently underperform their softmax-based counterparts in practice, especially in vision tasks. Closing this performance gap remains a central open problem.

Previous approaches primarily attributes this gap to the design of kernel feature maps $\phi(\cdot)$. To ensure numerical stability and avoid gradient explosion, most linear attention formulations impose a non-negativity constraint on feature maps, commonly enforced via *axis-aligned activations* such as ReLU (Cai et al., 2023; Han et al.,

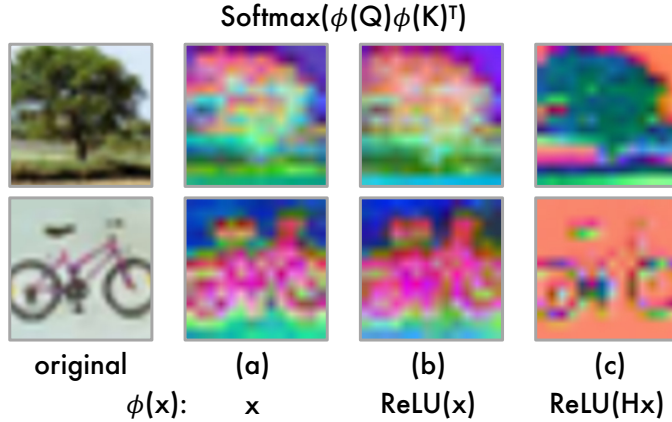


Figure 1 PCA Visualization of Feature Topology. We visualize $\text{Softmax}(\phi(\mathbf{Q})\phi(\mathbf{K})^\top)$ under constant normalization across three paradigms: (a) *Vanilla Attention*, $\phi(\mathbf{x}) = \mathbf{x}$ or \mathbf{Hx} ; (b) *Passive Truncation* $\phi(\mathbf{x}) = \text{ReLU}(\mathbf{x})$ results in “dead” dimension and information loss; (c) *Active Reorientation*, $\phi(\mathbf{x}) = \text{ReLU}(\mathbf{Hx})$ employs an isometric Householder reflection. This aligns informative features with the positive orthant, recovering the rich structural details lost in (b).

2023), $1 + \text{ELU}$ (Katharopoulos et al., 2020), or exponential mappings (Nahshan et al., 2024). While effective for stability, these kernels inherently discard negative feature components, triggering a “dead dimension” crisis that severely limits representational capacity. Some efforts attempt to mitigate the information loss caused by strict feature mapping, for instance, Hedgehog (Zhang et al., 2024) employs MLP-exp based mappings, while Polaformer (Meng et al., 2025) and Nalaformer (Anonymous, 2026) explore sign-decomposition and cosine similarity. However, they often rely on expanding the feature dimension d by k times, which paradoxically raise the computational cost to $\mathcal{O}(k^2d^2)$ and undermines the efficiency advantage of LA.

We argue that the such a limitation lies not in the non-negativity constraint itself, but in the rigidity of its enforcement. Crucially, attention similarity is based on the inner product $\langle \mathbf{q}, \mathbf{k} \rangle$, which is rotation invariant. Therefore, preserving similarity does not require preserving the original coordinate axes. Instead of *passively* truncating negative components, we hypothesize that one can *actively* reorient the feature space such that rotaing information-rich directions into the non-negative orthant before truncation.

To validate this hypothesis, we conduct a controlled PCA visualization of feature maps in Fig. 1, comparing standard ReLU truncation against a *rotation-augmentation* mapping. We implement this rotation via a Householder reflection \mathbf{H} , chosen for its strict *isometric* (Grigori and Timsit, 2024) property ($\langle \mathbf{Hq}, \mathbf{Hk} \rangle = \langle \mathbf{q}, \mathbf{k} \rangle$). A critical observation emerges: compared to the standard attention (a), the ReLU feature map (b) results in a *blurred* and sparse approximation, showing that passive truncation indiscriminately discards the fine-grained contrast details. In contrast, the reflected map (c) produces a distribution that is visually *distinct* yet structurally rich. This confirms that the information loss in LA is not inevitable; by transforming the non-negativity constraint from a destructive filter into a controllable geometric operation, we can restore the latent structural integrity typically discarded by axis-aligned clipping.

Motivated by these observations, we propose **MirrorLA**, a linear attention framework that shifts the paradigm from *passive clipping* to *active reorientation*. MirrorLA adopts a hierarchical design based on learnable Householder reflections to optimize feature topology at local, dynamic and global levels. At the *single-head* level, MirrorLA enables precise geometric control of full-rank rotation by decomposing high-dimensional feature space into disjoint 2D subspaces. We then apply strictly isometric Householder reflections within each block to align information-bearing directions into the non-negative orthant without altering pairwise distances. To avoid mirroring features into overly narrow subspace and trigger feature collapse in long-context modeling, we make the reflection *variance-conditioned*: the reflection angle is coupled to the block-wise signal variance, inducing a dynamic perturbation that yields a theoretical lower bound on activation diversity. This mitigates the dead-zone effect, where clustered tokens in low-variance regimes are indiscriminately truncated by static non-negativity boundaries. To overcome the rank fragmentation inherent in independent multi-head

processing (Zhou et al., 2025; Wang et al., 2025), we extend MirrorLA to the global scale via a unified *cross-head reflection*. This global operator couples feature spaces across heads through covariance mixing, allowing dormant subspaces to inherit discriminative structure from informative heads and improving overall expressivity.

We evaluate our method on five vision benchmarks across nine datasets, covering image classification, detection and segmentation, semantic segmentation, diffusion models, and ultra-long sequence super-resolution. Our model consistently outperforms baselines, with gains of up to 4.4% on classification, 4.7% on detection and segmentation, and a 6.6 mIoU improvement on semantic segmentation under lower FLOPs. Notably, for ultra-long sequence super-resolution, it achieves higher accuracy while reducing memory by up to 81.4% and inference time by up to 78%, and also yields lower FID in diffusion tasks.

2 Related Work

Efficient Sequential Vision Models. Treating images as token sequences has become a standard approach in modern vision architectures, inspired by the success of Transformer models in natural language processing (Vaswani et al., 2017). Vision Transformer (ViT) (Dosovitskiy et al., 2021) demonstrates that patchified images can be processed by self-attention to capture long-range dependencies, but its reliance on softmax attention incurs quadratic computational and memory costs, which quickly become prohibitive for high-resolution vision tasks. To mitigate this issue, a line of research focuses on improving the efficiency of Transformer-based vision models while largely preserving the attention formulation. DeiT (Touvron et al., 2021) leverages distillation strategies to enhance data efficiency, and Swin Transformer (Liu et al., 2021, 2022) restricts attention to shifted local windows, enabling scalable training while maintaining cross-window information flow. These methods primarily reduce constant factors or constrain attention scope, rather than fundamentally resolving the quadratic complexity of softmax attention. More recent efforts explore alternatives beyond standard attention mechanisms to further improve scalability. State space models (SSMs) have been adapted to vision by sequentially processing patch tokens, with VMamba (Liu et al., 2024; Huang et al., 2024) adopting raster-scan ordering to model spatial dependencies under linear-time complexity. In a different vein, VHeat (Wang et al., 2024) formulates visual representation learning as a diffusion-like process and models patch interactions through heat conduction, achieving sub-quadratic complexity via discrete cosine transform (DCT)-based operations.

Linear Attention. Linear attention reduces the quadratic complexity of softmax attention by replacing the exponential similarity with kernelized feature maps, enabling associative reordering and linear-time computation (Katharopoulos et al., 2020). Early approaches focus on approximating softmax using separable kernels, with representative designs based on ReLU (Han et al., 2023; Cai et al., 2023), exp (Nahshan et al., 2024). Performer (Choromanski et al., 2021) utilizes Random Fourier Features (RFF) to provide an unbiased estimate of the softmax kernel, while CosFormer (Qin et al., 2022) employs a linearithmic complexity approach with a ReLU-based kernel and cosine re-weighting to enforce locality. Linformer (Verma, 2021) approximates the self-attention matrix via low-rank decomposition, projecting the key and value sequences into a lower-dimensional subspace to achieve linear complexity. Beyond kernel selection, recent methods further introduce data-dependent modulation or gating mechanisms to stabilize large-scale training (Qin et al., 2024; MiniMax et al., 2025). While effective, such approaches still rely on fixed geometric parameterizations and do not explicitly address the information loss induced by kernelization. From a theoretical perspective, PolaFormer (Meng et al., 2025) mitigates information loss from non-negative feature maps via sign-aware inner product decomposition and using power function to lower the attention entropy. SAGA (Cao and Wang, 2025) and RALA (Fan et al., 2025b) exploit the property of the Hadamard product to enhance the intermediate matrices, thereby alleviating the low-rank bottleneck in linear attention. In-Line (Han et al., 2024a) shows that softmax attention is injective under mild conditions, which is generally not in linear attention, and MALA (Fan et al., 2025a) and NaLaFormer (Anonymous, 2026) also link this gap to information loss induced by non-negative feature maps. Consequently, while existing studies strive to preserve non-negativity, they largely overlook the fact that conventional activations as *passive truncation* mechanisms, incurring severe information loss and limiting the representational capacity of linear attention.

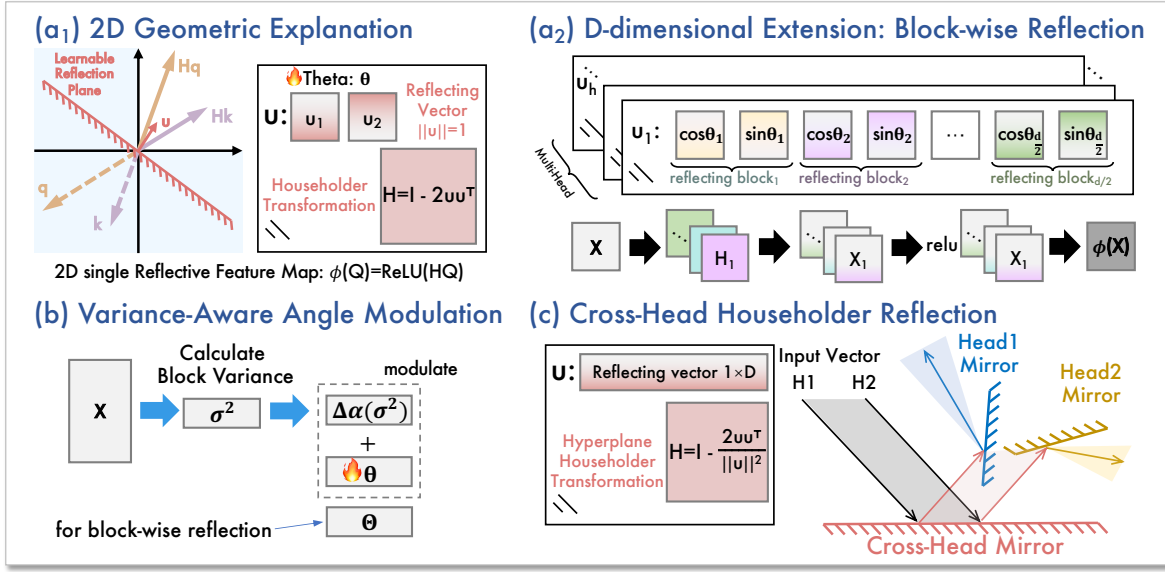


Figure 2 Overview of the MirrorLA framework. (a1) In 2D, a learnable Householder reflection \mathbf{H} reorients features \mathbf{Hq} \mathbf{Hk} before applying an axis-aligned non-negativity map, converting passive truncation into active alignment while preserving inner products by isometry. (a2) Extension to D -dim via block-wise and reflection with low overhead (b) Adaptively adjusting reflection angles based on block variance σ^2 to enhance feature diversity. (c) A global transformation before head-wise decomposition to encourage inter-head communication.

3 Method

The Information Loss of Linear Attention. Given an input sequence of length N and dimension d , Query (\mathbf{Q}), Key (\mathbf{K}), and Value (\mathbf{V}) matrices are in $\mathbb{R}^{N \times d}$. Standard attention computes pairwise similarities via:

$$\mathbf{o}_t = \sum_{i=1}^N \frac{\exp(\mathbf{q}_t \mathbf{k}_i^\top / \sqrt{d})}{\sum_{j=1}^N \exp(\mathbf{q}_t \mathbf{k}_j^\top / \sqrt{d})} \mathbf{v}_i, \quad (1)$$

which results in $\mathcal{O}(N^2d)$ complexity. To alleviate this, Linear Attention (LA) re-formulates the attention mechanism by replacing the softmax-normalized dot product with a generalized kernel function $\text{sim}(\mathbf{q}, \mathbf{k}) = \phi_r(\mathbf{q})\phi_r(\mathbf{k})^\top$. By leveraging the associative property of matrix multiplication, the complexity can be reduced to $\mathcal{O}(Nd^2)$ as

$$\mathbf{o}_t = \frac{\sum_{i=1}^N \phi_r(\mathbf{q}_t)\phi_r(\mathbf{k}_i)^\top \mathbf{v}_i}{\sum_{j=1}^N \phi_r(\mathbf{q}_t)\phi_r(\mathbf{k}_j)^\top} = \frac{\phi_r(\mathbf{q}_t) \sum_{i=1}^N \phi_r(\mathbf{k}_i)^\top \mathbf{v}_i}{\phi_r(\mathbf{q}_t) \sum_{j=1}^N \phi_r(\mathbf{k}_j)^\top}. \quad (2)$$

However, a critical constraint in this formulation is that the choice of the kernel feature map $\phi_r(\cdot)$ must ensure *non-negativity* $\text{sim}(\mathbf{q}, \mathbf{k}) \geq 0$. Otherwise, the denominator $\phi(\mathbf{q}) \sum \phi(\mathbf{k}_j)^\top$ will approach zero, resulting in numerical instability and gradient explosion during training. To satisfy this for arbitrary data distributions of \mathbf{Q} and \mathbf{K} , previous methods typically employ *axis-aligned* mappings such as $\text{ReLU}(\cdot)$ or $\exp(\cdot)$ to constrain the feature maps to the non-negative orthant. Despite their simplicity, such projections act as a hard thresholding operator and indiscriminately *suppress* features in the negative domain (as depicted in Fig.2), leading to irreversible information loss that hampers the model’s expressive capacity.

Overview of MirrorLA. To resolve the conflict between the non-negativity constraint and information preservation, we propose MirrorLA. Drawing on deep geometric isometries (Mhammedi et al., 2017), MirrorLA introduces a learnable reflection-based mechanism. Rather than passively *truncating* negative features, we optimally *reorient* the feature geometry into the non-negative orthant via Householder transformations prior

to activation so that the QK interactions can be steadily preserved. MirrorLA comprises three components: (1) *Block-wise Householder isometries* for local feature preservation (Sec. 3.1); (2) *Variance-aware modulation* to counteract oversmoothing in long-context modeling (Sec. 3.1); (3) *Cross-head reflection* to enable inter-head communications and global covariance mixing (Sec. 3.3).

3.1 Block-wise Householder Isometries

Householder Transformation. To preserve feature magnitude while satisfying non-negativity, we employ Householder reflections. The Householder matrix associated with a unit mirror vector $\mathbf{u} \in \mathbb{R}^d$ defines a reflection across the hyperplane orthogonal to \mathbf{u} :

$$\mathbf{H}_{\mathbf{u}} = \mathbf{I} - 2 \frac{\mathbf{u}\mathbf{u}^T}{\|\mathbf{u}\|_2^2}. \quad (3)$$

This transformation is orthogonal ($\mathbf{H}_{\mathbf{u}}^T \mathbf{H}_{\mathbf{u}} = \mathbf{I}$), ensuring it is an isometry that preserves Euclidean norms. Accordingly, the reflection of an input vector \mathbf{x} with respect to this hyperplane is obtained as $\mathbf{H}_{\mathbf{u}}\mathbf{x}$. We first show a simplified 2D case to build a geometric interpretation:

2D Case: Intuition of Mirrored Feature Map. Let the mirror vector $\mathbf{u} = [u_1, u_2]^T \in \mathbb{R}^2$ be a unit mirror vector and the input be $\mathbf{x} \in \mathbb{R}^2$. The corresponding Householder reflection is:

$$\tilde{\mathbf{x}} = \mathbf{H}_{\mathbf{u}}\mathbf{x}, \quad \mathbf{H}_{\mathbf{u}} = \mathbf{I} - 2\mathbf{u}\mathbf{u}^T, \quad (4)$$

where $\|\mathbf{u}\|_2 = 1$. Parameterizing \mathbf{u} by an angle θ ,

$$u_1 = \cos \theta, \quad u_2 = \sin \theta. \quad (5)$$

we obtain the closed form 2D Householder formula as

$$\mathbf{H}_{\mathbf{u}} = \begin{bmatrix} 1 - 2u_1^2 & -2u_1u_2 \\ -2u_1u_2 & 1 - 2u_2^2 \end{bmatrix} = \begin{bmatrix} \cos 2\theta & \sin 2\theta \\ \sin 2\theta & -\cos 2\theta \end{bmatrix}. \quad (6)$$

Thus, in two dimensions, the Householder transformation can be interpreted as a reflection across a line with angle θ , providing an intuitive view of how the input is mirrored before further non-negative mapping such as ReLU, which is defined as,

$$\phi_r(\mathbf{x}) = \text{ReLU}(\mathbf{H}_{\mathbf{u}}\mathbf{x}) \quad (7)$$

As shown in Fig. 2 (left), a learnable unit vector \mathbf{u} parameterized by an angle θ allows the model to optimally rotate the mirror geometry relative to the ReLU activation boundary. Instead of passive truncation, the elements are reflected into the active region, preserving structural information that would otherwise be discarded. Consequently, the reflected features retain richer information and display more balanced statistics, which enhances the expressiveness of the feature map and yields more *stable* linear attention estimation.

Extension to High-Dimension: Block-wise Reflection. To scale this to arbitrary dimensions D efficiently, we partition the query or key feature vector $\mathbf{x} \in \mathbb{R}^D$ into $M = D/2$ disjoint two-dimensional blocks:

$$\mathbf{x} = [\mathbf{x}_1, \mathbf{x}_2, \dots, \mathbf{x}_M], \quad \mathbf{x}_m \in \mathbb{R}^2. \quad (8)$$

For each block m , we associate a learnable mirror vector $\mathbf{u}_m = [\cos \theta_m \ \sin \theta_m]$ and reflect each block independently:

$$\mathbf{H}_m = \mathbf{I}_2 - 2\mathbf{u}_m(\mathbf{u}_m)^T, \quad \tilde{\mathbf{x}}_m = \mathbf{H}_m\mathbf{x}_m, \quad (9)$$

Stacking the reflected blocks gives the full transformed vector, which is followed by ReLU to enforce non-negativity:

$$\phi_r(\mathbf{x}) = \text{ReLU}(\tilde{\mathbf{x}}), \quad \tilde{\mathbf{x}} = [\tilde{\mathbf{x}}_1, \dots, \tilde{\mathbf{x}}_M] \in \mathbb{R}^D. \quad (10)$$

Given a query \mathbf{q} and key \mathbf{k} , their linear attention kernel is computed in a blockwise *additive* manner. For each head h , we evaluate the similarity by summing contributions from all 2D blocks:

$$\langle \phi_r(\mathbf{q}), \phi_r(\mathbf{k}) \rangle = \sum_{m=1}^M \langle \phi_r(\mathbf{q}_m), \phi_r(\mathbf{k}_m) \rangle, \quad (11)$$

which is equivalent to the standard inner product over \mathbb{R}^D but explicitly decomposed into 2D reflective components. This block-wise design imposes a local mixing bias, reorienting features within small coordinate groups rather than globally entangling all dimensions. This yields stable geometry adaptation with $\mathcal{O}(d)$ complexity and bounded operator norm inherited from orthogonal reflection.

3.2 Rotating the Mirror: Variance-Aware Angle Modulation

While block-wise reflections optimize static geometry, long-context modeling suffers from *feature oversmoothing*, where token embeddings concentrate in a narrow subspace. If the reflection angle θ_m is static, these aligned tokens may all map to the same sign pattern, causing the subsequent ReLU to zero-out entire sequence segments identically.

To mitigate this, we introduce a *variance-aware angle modulation* mechanism that *adaptively* perturbs the reflection angle based on the block variance σ_m^2 across the sequence length L , encouraging activation-pattern diversity in low-variance subspaces. Let $\mathbf{x}_{t,m} \in \mathbb{R}^2$ denote the feature vector of block m at token t , and let $\bar{\mathbf{x}}_m = \frac{1}{L} \sum_{t=1}^L \mathbf{x}_{t,m}$ be the empirical mean. We define the block-level variance as

$$\sigma_m^2 = \frac{1}{2L} \sum_{t=1}^L \|\mathbf{x}_{t,m} - \bar{\mathbf{x}}_m\|^2. \quad (12)$$

Intuitively, a small σ_m^2 indicates that token representations within this block carry weak token-specific information, and thus benefit from a stronger reorientation relative to the activation boundary. We accordingly modulate the reflection angle by:

$$\Theta_m = \theta_m + \Delta\alpha(\sigma^2), \quad (13)$$

$$\Delta\alpha(\sigma^2) = \text{sigmoid}\left(\frac{\lambda}{\sigma_m^2 + \varepsilon}\right) \cdot \alpha_{\max}, \quad (14)$$

where θ_m denotes the learnable base reflection angle for block m , $\alpha_{\max} \in \{\pi/8, \pi/4, \pi/2\}$ is a scaling hyperparameter controlling the maximum perturbation, λ controls the variant sensitivity, and ε is a small constant for numerical stability. We then replace θ_m with the variance-aware angle Θ_m in the Householder reflection, while keeping the per-block computation linear in D .

Theoretical Motivation. The following theorem formalizes how this modulation promotes activation diversity.

Theorem 3.1: Collapse-aware Activation Diversification

Let $\mathcal{X} = \{\mathbf{x}_{t,m}\}_{t=1}^L \subset \mathbb{R}^2$ be the token features of a 2D block with empirical variance σ^2 computed over the token dimension. Consider the modulated mirror map

$$\phi(x; \Theta) = \text{ReLU}(\mathbf{H}_m(\Theta_m)\mathbf{x}_{t,m}), \quad (15)$$

where $\Delta\alpha(\sigma^2) = \text{sigmoid}(1/(\sigma^2 + \varepsilon)) \cdot \alpha$ and $\mathbf{H}(\Theta_m)$ denotes a 2D Householder reflection parameterized by angle Θ_m (Eq. 13). Define the binary activation mask:

$$s(\mathbf{x}_{t,m}; \Theta_m) = \mathbb{I}[\mathbf{H}(\Theta_m)\mathbf{x}_{t,m} > \mathbf{0}] \in \{0, 1\}^2. \quad (16)$$

Then, in the low-variance regime $\sigma^2 \rightarrow 0$, the modulation saturates $\Theta_m \rightarrow \theta + \alpha_{\max}$ and induces a non-degenerate reorientation of the reflection hyperplane. In particular, for perturbative tokens $\mathbf{x}_{t,m} = \bar{\mathbf{x}}_m + \delta_t$,

the expected mask disagreement satisfies

$$\begin{aligned} & \mathbb{E}_{t \neq t'} [\|s(\mathbf{x}_{t,m}; \Theta) - s(\mathbf{x}_{t',m}; \Theta)\|_0] \\ & \geq c(\bar{\mathbf{x}}_m, \Theta) \cdot \mathbb{E}_{t \neq t'} [\|\mathbf{x}_{t,m} - \mathbf{x}_{t',m}\|_2], \end{aligned} \quad (17)$$

for some $c(\bar{\mathbf{x}}, \Theta_m) > 0$ whenever $\mathbf{H}(\Theta_m)\bar{\mathbf{x}}$ lies within a bounded margin of the ReLU boundary.

Proof sketch. As $\sigma^2 \rightarrow 0$, we have $1/(\sigma^2 + \varepsilon) \rightarrow \infty$, hence $\Delta\alpha(\sigma^2)$ saturates near α_{\max} , yielding the maximal angular shift. Mask disagreement arises when tokens fall on different sides of the coordinate hyperplanes after reflection, which is controlled by the distance (margin) of $\mathbf{H}(\Theta_m)\bar{\mathbf{x}}$ to the ReLU boundary. By rotating the reflection hyperplane in the low-variance regime, the proposed modulation prevents an entire oversmoothed token cluster from sharing an identical activation pattern, thereby mitigating collapse under long-context accumulation. \square

3.3 Cross-Head Householder Reflection

While multi-head factorization improves expressivity, purely head-wise processing implicitly limits interactions across heads and can lead to fragmented representations, especially under non-negative feature maps. Recent studies on *inter-head communication* (Zhou et al., 2025; Wang et al., 2025) suggest that lightweight transformations along the head dimension H can substantially enhance attention capacity by allowing heads to exchange complementary information. Motivated by this perspective, we introduce a global cross-head Householder reflection that couples the full feature space *before* head-wise decomposition, enabling global correlation mixing with stable conditioning.

Formally, let $\mathbf{X} \in \mathbb{R}^{L \times HD}$ denote the concatenated multi-head features, where H is the number of heads and D is the per-head dimension. We apply a global Householder reflection

$$\phi_c(\mathbf{X}) = \mathbf{X}\mathbf{H}_c, \quad \mathbf{H}_c = \mathbf{I}_{HD} - 2 \frac{\mathbf{u}_c \mathbf{u}_c^\top}{\|\mathbf{u}_c\|_2^2}, \quad (18)$$

where $\mathbf{u}_c \in \mathbb{R}^{HD}$. Importantly, the transformation preserves the Euclidean geometry while introducing controlled cross-head mixing.

Covariance Mixing. Let $\Sigma = \text{Cov}(\mathbf{X}) \in \mathbb{R}^{HD \times HD}$ denote the covariance of the concatenated head features at a token. Since \mathbf{H}_c is orthogonal, the reflected covariance satisfies,

$$\Sigma' = \text{Cov}(\mathbf{X}\mathbf{H}_c) = \mathbf{H}_c^\top \Sigma \mathbf{H}_c, \quad (19)$$

which preserves the covariance spectrum but generally redistributes correlation mass across head blocks. As a result, $\phi_c(\cdot)$ mitigates the block-diagonal bias induced by independent head processing, allowing low-variance (“dead”) heads to recover discriminative directions from high-variance heads prior to the subsequent head-wise non-negative mapping. After the cross-head reflection, $\phi_c(\mathbf{X})$ is reshaped back into H heads and processed with the variance-aware block-wise Householder reflections from §3.2, followed by ReLU per head. The complete MirrorLA pipeline is summarized in Algorithm 1.

4 Experiments

In this section, we conduct extensive experiments to evaluate the effectiveness of MirrorLA including image classification, object detection and instance segmentation, diffusion transformer and high-resolution dense prediction tasks such as semantic segmentation and super-resolution.

4.1 Image Classification on ImageNet-1K

Settings. On ImageNet-1K (Deng et al., 2009), we evaluate MirrorLA by training from scratch and reporting Top-1 accuracy. To provide a comprehensive evaluation, we compare our method against various State-of-the-Art (SOTA) efficient vision models. For a fair and structured analysis, these baselines are categorized into

Algorithm 1 Reflecting Feature Map

```

# x: input features [B, N, D]
# H: number of heads, d = D / H

# ----- Global reflection -----
u_c = normalize(randn(D))
x = x - 2 * u_c * <x, u_c>
# ----- Head-wise reshape -----
x = reshape(x, [B, H, N, d])
# ----- Block partition -----
x_blk = reshape(x, [B, H, N, d//2, 2])
# ----- Variance-aware angle modulation -----
theta = (randn(H, d//2)
var = Var(x_blk over N and 2D)
delta = sigmoid(lambda / (var + epsilon)) * alpha_max
theta = theta + delta
# ----- Block-wise reflection -----
u = [cos (theta), sin (theta)]
x_blk = x_blk - 2 * u * <x_blk, u>
# ----- Restore shape -----
x = reshape(x_blk, [B, H, N, D])
return ReLU(x)

```

several tiers based on parameter count, allowing for direct performance comparisons within similar model scales.

Results. The results in Tab. 1 demonstrate that MirrorLA consistently delivers strong and scalable performance across model sizes. At the tiny scale, MirrorLA-T achieves 82.8% Top-1 accuracy, improving upon RAVLT-T by 0.2% and RMT-T by 0.4%, indicating clear gains even in low-capacity regimes. As model capacity increases, the performance advantage becomes more stable. MirrorLA-S reaches 84.2%, surpassing RMT-S by 0.1%, while MirrorLA-B further improves to 85.3%, exceeding RAVLT-B by 0.2%. At the largest scale, MirrorLA-L attains 85.7% Top-1 accuracy, outperforming both RMT-L and RAVLT-L, which highlights the effectiveness of MirrorLA in leveraging increased model capacity. Overall, these results suggest that MirrorLA not only provides consistent improvements over prior methods but also scales favorably across different model sizes.

4.2 Object Detection and Instance Segmentation

Settings. We evaluate MirrorLA on COCO (Lin et al., 2014) dataset for object detection and instance segmentation. By integrating MirrorLA into RetinaNet (Lin et al., 2017) and Mask R-CNN (He et al., 2017) under both $1\times$ and $3\times$ training schedules. For fair comparison, we adopt the evaluation protocol of FL-Transformer (Han et al., 2023).

Results. As shown in Tab. 2, MirrorLA consistently improves detection and instance segmentation performance under comparable computational budgets. Specifically, MirrorLA yields up to 1.8 AP^b gains for RetinaNet, while for Mask R-CNN it improves AP^b from 47.2 to 49.9 under the $1\times$ schedule and from 50.7 to 51.3 under the $3\times$ schedule.

4.3 Semantic Segmentation

Settings. We integrate MirrorLA into semantic segmentation on ADE20K (Zhou et al., 2019) and Cityscapes (Cordts et al., 2016), using mIoU as the evaluation metric. We initialize the backbone with ImageNet-1K pretrained weights and train the segmentation models using the *mmcv-segmentation* framework (Contributors, 2018), following common practice in recent works (Guo et al., 2022b; Cai et al., 2023). Additionally, we adopt an FPN decoder with other linear attention methods in Appendix Tab. 9.

Results. MirrorLA consistently raises mIoU under similar computational budgets on both datasets. As shown in Tab. 3, MirrorLA delivers stronger segmentation accuracy with competitive complexity. On ADE20K, MirrorLA-T and MirrorLA-S obtain 48.8 and 50.9 mIoU, outperforming EfficientViT-B2 (Cai et al., 2023) at 45.9 and EfficientViT-L1 (Cai et al., 2023) at 49.2. On Cityscapes, MirrorLA-T reaches 82.5 mIoU and MirrorLA-S further improves to 83.5, exceeding SegNeXt-S (Guo et al., 2022b) at 81.3 and EfficientViT-B3

Table 1 Comparison of the ImageNet-1K classification with the SOTA efficient models. The “PARAMS” column represents the number of parameters, “Acc” for Top-1 accuracy.

MODEL	PARAMS	FLOPs	ACC.
Conv2Former-N (Hou et al., 2024)	15M	2.2G	81.5
RMT-T (Fan et al., 2024)	14M	2.5G	82.4
Agent-PVT-T (Han et al., 2024c)	12M	2.0G	78.4
RMT-T (Fan et al., 2024)	14M	2.5G	82.4
RAVLT-T (Fan et al., 2025b)	15M	2.6G	82.6
MirrorLA-T	15M	2.6G	82.8
Conv2Former-T (Hou et al., 2024)	27M	4.4G	83.2
MambaOut-T (Yu and Wang, 2025)	27M	4.5G	82.7
VMamba-T (Liu et al., 2024)	30M	4.9G	82.6
Agent-Swin-T (Han et al., 2024c)	29M	4.5G	82.6
Vim-S (Zhu et al., 2024)	26M	3.7G	80.6
VMamba-T (Liu et al., 2024)	30M	4.9G	82.6
LocalVMamba-T (Huang et al., 2024)	26M	5.7G	82.7
MOAT-0 (Yang et al., 2023)	28M	5.7G	83.3
Pola-Swin-T (Meng et al., 2025)	29M	4.5G	82.6
ViG-H-T (Liao et al., 2025)	29M	4.5G	82.8
MILA-T (Han et al., 2024b)	25M	4.2G	83.5
MirrorLA-S	26M	4.9G	84.2
MambaOut-S (Yu and Wang, 2025)	49M	9.0G	84.1
MogaNet-B (Li et al., 2024)	44M	10G	84.3
VMamba-S (Liu et al., 2024)	50M	8.7G	83.6
StructViT-B-8-1 (Kim et al., 2024)	52M	12G	84.3
SOFT-L (Lu et al., 2024)	64M	11G	83.1
FL-Swin-S (Han et al., 2023)	51M	8.7G	83.5
Agent-Swin-S (Han et al., 2024c)	50M	8.7G	83.7
Pola-Swin-S (Meng et al., 2025)	50M	8.7G	83.6
ViG-H-S (Liao et al., 2025)	50M	8.8G	83.8
RMT-B (Fan et al., 2024)	54M	9.7G	85.0
MILA-S (Han et al., 2024b)	43M	7.3G	84.4
RAVLT-B (Fan et al., 2025b)	48M	10.6G	85.1
MirrorLA-B	48M	10.6G	85.3
MambaOut-B (Yu and Wang, 2025)	85M	15.8G	84.2
VMamba-B (Liu et al., 2024)	89M	15.4G	83.9
FL-Swin-B (Han et al., 2023)	89M	15.4G	83.8
Agent-Swin-B (Han et al., 2024c)	88M	15.4G	84.0
Pola-Swin-B (Meng et al., 2025)	88M	15.4G	83.8
SMT-L (Lin et al., 2023)	81M	17.7G	84.6
VRWKV-B (Duan et al., 2025)	94M	18.2G	82.0
ViG-H-B (Liao et al., 2025)	89M	15.5G	84.2
MaxViT-B (Tu et al., 2022)	120M	23.4G	84.9
GC-ViT-B (Hatamizadeh et al., 2023)	90M	14.8G	85.0
RMT-L (Fan et al., 2024)	95M	18.2G	85.5
InLine-Swin-B (Han et al., 2024a)	88M	15.4G	82.0
MILA-B (Han et al., 2024b)	96M	16.2G	85.3
RAVLT-L (Fan et al., 2025b)	95M	17.3G	85.5
MirrorLA-L	95M	17.3G	85.7

(Cai et al., 2023) at 83.0. As shown in Fig. 3 (left), MirrorLA produces noticeably cleaner and more precise semantic boundaries compared to EfficientViT and SegNext. It better separates adjacent objects, accurately captures small details such as traffic signs, and reduces misclassified or missing regions, leading to improved overall segmentation quality.

Table 2 Object detection and instance segmentation results on the COCO dataset. The “P” column represents the number of parameters, and “F” for FLOPs.

MODEL	P (M)	F (G)	RETINANET 1×					
			AP ^b	AP ₅₀ ^b	AP ₇₅ ^b	AP _S ^b	AP _M ^b	AP _L ^b
PVT-T (Wang et al., 2022)	23	221	39.4	59.8	42.0	25.5	42.0	52.1
MPViT-XS (Lee et al., 2022)	20	211	43.8	65.0	47.1	28.1	47.6	56.5
SOFT++ T (Lu et al., 2024)	23	200	41.9	62.7	44.7	27.8	45.4	55.6
RMT-T (Fan et al., 2024)	23	199	45.1	66.2	48.1	28.8	48.9	61.1
RAVLT-T (Fan et al., 2025b)	24	201	44.1	64.3	47.4	26.4	48.1	59.3
MirrorLA-T	24	200	46.1	67.4	49.4	28.8	50.4	61.7
Swin-T (Liu et al., 2021)	38	248	41.7	63.1	44.3	27.0	45.3	54.7
MPViT-S (Lee et al., 2022)	32	248	45.7	57.3	48.8	28.7	49.7	59.2
PVTv2-B2 (Wang et al., 2022)	35	290	44.6	65.6	47.6	27.4	48.8	58.6
CMT-S (Guo et al., 2022a)	44	231	44.3	65.5	47.5	27.1	48.3	59.1
RAVLT-T (Fan et al., 2025b)	44	262	46.7	67.2	50.4	31.4	51.1	62.3
MirrorLA-S	34	243	48.5	69.8	52.2	32.2	52.9	63.7
MODEL	P (M)	F (G)	MASK R-CNN 1×					
			AP ^b	AP ₅₀ ^b	AP ₇₅ ^b	AP ^m	AP ₅₀ ^m	AP ₇₅ ^m
PVTv2-b1 (Wang et al., 2022)	33	243	41.8	54.3	45.9	38.8	61.2	41.6
MPViT-XS (Lee et al., 2022)	30	231	47.3	69.1	51.9	42.7	66.2	46.0
FL-PVT-T (Han et al., 2023)	32	244	38.2	61.6	41.9	37.0	57.6	39.0
RAVLT-T (Fan et al., 2025b)	33	219	47.2	69.1	51.7	42.7	66.0	46.0
MirrorLA-T	33	219	47.7	69.6	52.6	43.0	66.6	46.2
InternImage-T (Wang et al., 2023)	49	270	47.2	69.0	52.1	42.5	66.1	45.8
MambaOut-T (Wang et al., 2023)	43	262	45.1	67.3	49.6	41.0	64.1	44.1
MPViT-S (Lee et al., 2022)	43	268	46.4	68.6	51.2	42.4	65.6	45.7
CMT-S (Guo et al., 2022a)	45	249	44.6	66.8	48.9	40.7	63.9	43.4
MILA-T (Han et al., 2024b)	44	262	46.8	69.5	51.5	42.1	66.4	45.0
MirrorLA-S	44	262	49.9	71.6	54.7	44.5	68.4	48.1
MODEL	P (M)	F (G)	MASK R-CNN 3×					
			AP ^b	AP ₅₀ ^b	AP ₇₅ ^b	AP ^m	AP ₅₀ ^m	AP ₇₅ ^m
XCiT-T12/8 (Ali et al., 2021)	26	266	44.5	66.4	48.8	40.4	63.5	43.3
RMT-T (Fan et al., 2024)	33	218	47.1	68.8	51.7	42.6	65.8	45.9
MPViT-T (Lee et al., 2022)	28	216	44.8	66.9	49.2	41.0	64.2	44.1
MirrorLA-T	33	129	49.4	70.7	54.3	44.1	67.7	47.7
InternImage-T (Wang et al., 2023)	49	270	49.1	70.4	54.1	43.7	67.3	47.3
RMT-S (Fan et al., 2024)	46	262	50.7	71.9	55.6	44.9	69.1	48.4
FL-Swin-T (Han et al., 2023)	49	268	46.5	68.5	50.8	42.1	65.4	45.1
VMamba-T (Liu et al., 2024)	50	270	48.9	70.6	53.6	43.7	67.7	46.8
MILA-T (Han et al., 2024b)	44	255	48.8	71.0	53.6	43.8	68.0	46.8
MirrorLA-S	44	262	51.3	72.3	56.4	45.4	69.6	49.0

Table 3 Semantic segmentation results compared with SOTA methods on ADE20K and Cityscapes benchmarks. FLOPs is calculated with input size 512×512 for ADE20K and 2,048×1,024 for Cityscapes.

METHOD	PARA	ADE20K		CITYSCAPES	
		MIOU	FLOPs	MIOU	FLOPs
VWFormer-B1 (Yan et al., 2024)	14M	44.0	13G	80.4	-
EfficientViT-B2 (Cai et al., 2023)	15M	45.9	9.1G	82.1	74G
SegFormer-B1 (Xie et al., 2021)	14M	42.2	16G	78.5	244G
SegNeXt-S (Xie et al., 2021)	15M	44.3	16G	81.3	125G
MirrorLA-T	14M	48.8	14G	82.5	110G
VRWKV-S (Duan et al., 2025)	29M	47.2	46G	-	-
MambaOut-T (Yu and Wang, 2025)	54M	47.4	-	-	-
VWFormer-B2 (Yan et al., 2024)	27M	48.1	47G	81.7	415G
EfficientViT-B3 (Cai et al., 2023)	40M	49.0	22G	83.0	179G
SegNeXt-B (Guo et al., 2022b)	28M	48.5	35G	82.6	276G
EfficientViT-L1 (Cai et al., 2023)	40M	49.2	36G	82.7	282G
SegFormer-B2 (Xie et al., 2021)	28M	46.5	62G	81.0	711G
MirrorLA-S	24M	50.9	25G	83.5	205G

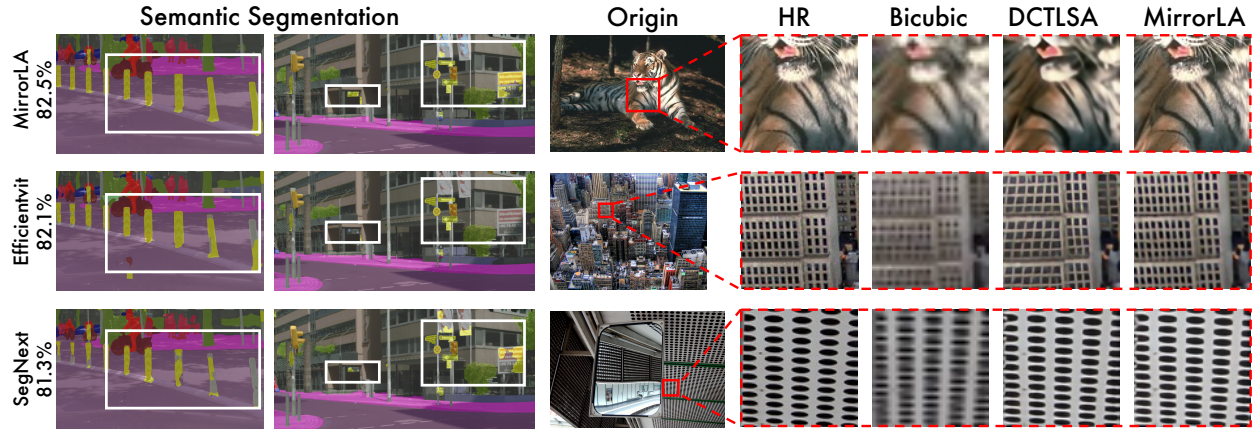


Figure 3 Visualization of Semantic Segmentation and Super-Resolution (SR) tasks. Left: Comparative results on the Cityscapes dataset, where MirrorLA achieves superior segmentation integrity, whereas competing methods suffer from incomplete masks. Right: Comparison of SR performance; MirrorLA reconstructs details more effectively, while DCTLSA introduces noticeable structural distortions.

4.4 Super Resolution

Settings. We evaluate MirrorLA on lightweight single-image super-resolution by integrating it into an efficient SR baseline, DCTLSA (Zeng et al., 2023). Following common practice, we consider $\times 3$ and $\times 4$ upscaling and report PSNR/SSIM on standard SR benchmarks. We additionally measure inference latency on an RTX 3090 to assess efficiency.

Results. Tab. 4 shows that integrating MirrorLA into DCTLSA consistently improves PSNR/SSIM for both $\times 3$ and $\times 4$ upscaling. For example, at $\times 4$, Set5 improves from 32.44/0.8973 to 32.53/0.8983, and Urban100 from 26.41/0.7944 to 26.65/0.8007. In addition, DCTLSA-MirrorLA significantly reduces latency and memory: on Manga109 $\times 4$, latency is reduced by over 75% and memory usage is cut by over 80%. As visualized in Fig. 3 (right), MirrorLA produces super-resolved images closer to the ground truth, with clear details and better structural preservation.

Table 4 Quantitative comparisons between MirrorLA and other lightweight image super-resolution methods. MEM. denotes GPU memory consumption, and LAT. denotes latency (per image).

MODEL	SCALE	SET5		SET14		BSDS100		URBAN100		MANGA109	
		PSNR	SSIM								
Bicubic	$\times 4$	28.42	0.8104	26.00	0.7027	25.96	0.6675	23.14	0.6577	24.89	0.7866
SwinIR (Liang et al., 2021)	$\times 4$	32.44	0.8976	28.77	0.7858	27.69	0.7406	26.47	0.7980	30.92	0.9151
DCTLSA (Zeng et al., 2023)	$\times 4$	32.44	0.8973	28.77	0.7846	27.67	0.7386	26.41	0.7944	31.04	0.9138
DCTLSA-MirrorLA	$\times 4$	32.53	0.8983	28.84	0.7867	27.74	0.7409	26.65	0.8007	31.30	0.9170
Bicubic	$\times 3$	30.39	0.8682	27.55	0.7742	27.21	0.7385	24.46	0.7349	26.95	0.8556
SwinIR (Liang et al., 2021)	$\times 3$	34.62	0.9289	30.54	0.8463	29.20	0.8082	28.66	0.8624	33.98	0.9478
DCTLSA (Zeng et al., 2023)	$\times 3$	34.76	0.9296	30.64	0.8474	29.27	0.8093	28.81	0.8674	34.42	0.9492
DCTLSA-MirrorLA	$\times 3$	34.84	0.9301	30.70	0.8488	29.33	0.8106	29.03	0.8688	34.61	0.9505
EFFICIENCY@3090		SCALE	LAT.	MEM.	LAT.	MEM.	LAT.	MEM.	LAT.	MEM.	LAT.
DCTLSA-Softmax	$\times 4$	57.70ms	1.05GB	109.04ms	1.47GB	72.06ms	0.59GB	349.86ms	4.28GB	456.71ms	3.44GB
DCTLSA-MirrorLA	$\times 4$	55.28ms	0.18GB	55.29ms	0.30GB	49.62ms	0.11GB	79.03ms	0.85GB	100.69ms	0.67GB
- SAVE	$\times 4$	4.2%	82.9%	49.3%	79.6%	31.1%	81.4%	77.4%	80.1%	78.0%	80.5%
DCTLSA-Softmax	$\times 3$	57.90ms	1.66GB	113.04ms	2.27GB	76.74ms	0.93GB	355.81ms	7.19GB	571.86ms	5.49GB
DCTLSA-MirrorLA	$\times 3$	46.11ms	0.33GB	51.82ms	0.51GB	42.70ms	0.19GB	146.27ms	1.52GB	183.47ms	1.20GB
- SAVE	$\times 3$	20.4%	80.1%	54.2%	77.5%	44.3%	79.6%	58.9%	78.9%	67.9%	78.1%

4.5 Diffusion Transformer

Settings. Diffusion transformers provide a suitable testbed for evaluating linear attention. Following DiT (Peebles and Xie, 2023) and SiT (Ma et al., 2024), we replace the attention module with MirrorLA and conduct experiments on ImageNet-1K (Deng et al., 2009) under the same training and evaluation protocols as the corresponding baselines.

Results. Tab. 5 reports that integrating MirrorLA consistently improves diffusion transformers across both DiT and SiT architectures. On the DiT branch, MirrorLADiT yields a sizable improvement over DiG (Zhu et al., 2025). Specifically, the FID decreases from 62.06 to 58.07 and the sFID decreases from 11.77 to 11.21, while the IS increases from 22.81 to 24.70. On the SiT branch, MirrorLASiT achieves the best overall performance. It attains lower FID and sFID values of 52.29 and 8.41, respectively, together with a higher IS of 28.51, and demonstrates strong precision and recall of 0.43 and 0.61. This performance surpasses both SiT (Ma et al., 2024) and EfficientSiT (Pu et al., 2024).

Table 5 Diffusion transformer results. MirrorLA achieves outstanding performance on both DiT and SiT.

MODEL	FID ↓	sFID ↓	IS ↑	PRECISION ↑	RECALL ↑
DiT (Peebles and Xie, 2023)	68.40	-	-	-	-
DiG (Zhu et al., 2025)	62.06	11.77	22.81	0.39	0.56
MirrorLADiT	58.07	11.21	24.70	0.41	0.59
SiT (Ma et al., 2024)	58.61	9.25	24.31	0.41	0.59
EfficientSiT (Pu et al., 2024)	53.57	9.01	27.26	0.43	0.61
MirrorLASiT	52.29	8.41	28.51	0.43	0.61

4.6 Ablation study

We evaluate MirrorLA on the Swin-T architecture following the protocol of FLatten-Transformer (Han et al., 2023) and compare it with existing linear attention mechanisms. As a modular enhancement inserted before the non-negativity constraint, our method surpasses existing linear attention variants with a 0.6% accuracy gain shown in Appendix Tab. 7. Additionally, we conduct extensive ablation studies further confirm the necessity of our hierarchical design: on the XT setting, disabling the full variant or removing cross-head reflection leads to performance drops of 0.5% and 0.3%, respectively. Detailed analyses regarding hyperparameter sensitivity (λ, α_{\max}) and component-wise performance are provided in the Appendix Tab. 8.

5 Conclusion

In this work, we introduce **MirrorLA**, a linear attention framework that replaces passive non-negativity clipping with active geometric reorientation via learnable Householder reflections. At the single-head level, we generalize 2D reflections to high-dimensional feature spaces through block-wise decomposition, and further propose Variance-Aware Angle Modulation to enable data-dependent mirror transformations. At the global scale, we design a unified cross-head reflection to enhance inter-head communication. Extensive experiments demonstrate that MirrorLA consistently achieves superior performance while substantially reducing memory footprint and time.

References

- Alaaeldin Ali, Hugo Touvron, Mathilde Caron, Piotr Bojanowski, Matthijs Douze, Armand Joulin, Ivan Laptev, Natalia Neverova, Gabriel Synnaeve, Jakob Verbeek, and Hervé Jégou. Xcit: Cross-covariance image transformers. In *Proc. Annual Conference on Neural Information Processing (NeurIPS)*, pages 20014–20027, 2021.
- Anonymous. Norm \times direction: Restoring the missing query norm in vision linear attention. *Proc. International Conference on Machine Learning (ICML) Submission*, 2026.
- Daniel Bolya, Cheng-Yang Fu, Xiaoliang Dai, Peizhao Zhang, and Judy Hoffman. Hydra attention: Efficient attention with many heads. In *Proc. European Conference on Computer Vision (ECCV)*, pages 35–49, 2022.
- Han Cai, Junyan Li, Muyan Hu, Chuang Gan, and Song Han. Efficientvit: Lightweight multi-scale attention for high-resolution dense prediction. In *Proc. International Conference on Computer Vision (ICCV)*, pages 17256–17267, 2023.
- Yuan Cao and Dong Wang. SAGA: selective adaptive gating for efficient and expressive linear attention. *CoRR*, abs/2509.12817, 2025.
- Krzysztof Marcin Choromanski, Valerii Likhoshesterov, David Dohan, Xingyou Song, Andreea Gane, Tamás Sarlós, Peter Hawkins, Jared Quincy Davis, Afroz Mohiuddin, Lukasz Kaiser, David Benjamin Belanger, Lucy J. Colwell, and Adrian Weller. Rethinking attention with performers. In *Proc. International Conference on Learning Representations (ICLR)*, 2021.
- MMCV Contributors. MMCV: OpenMMLab computer vision foundation. <https://github.com/open-mmlab/mmcv>, 2018.
- Marius Cordts, Mohamed Omran, Sebastian Ramos, Timo Rehfeld, Markus Enzweiler, Rodrigo Benenson, Uwe Franke, Stefan Roth, and Bernt Schiele. The cityscapes dataset for semantic urban scene understanding. In *Proc. IEEE Conference on Computer Vision and Pattern Recognition (CVPR)*, pages 3213–3223, 2016.
- Jia Deng, Wei Dong, Richard Socher, Li-Jia Li, Kai Li, and Li Fei-Fei. Imagenet: A large-scale hierarchical image database. In *Proc. IEEE Conference on Computer Vision and Pattern Recognition (CVPR)*, pages 248–255, 2009.
- Alexey Dosovitskiy, Lucas Beyer, Alexander Kolesnikov, Dirk Weissenborn, Xiaohua Zhai, Thomas Unterthiner, Mostafa Dehghani, Matthias Minderer, Georg Heigold, Sylvain Gelly, Jakob Uszkoreit, and Neil Houlsby. An image is worth 16x16 words: Transformers for image recognition at scale. In *Proc. International Conference on Learning Representations (ICLR)*, 2021.
- Yuchen Duan, Weiyun Wang, Zhe Chen, Xizhou Zhu, Lewei Lu, Tong Lu, Yu Qiao, Hongsheng Li, Jifeng Dai, and Wenhui Wang. Vision-rwkv: Efficient and scalable visual perception with rwkv-like architectures. In *Proc. International Conference on Learning Representations (ICLR)*, 2025.
- Qihang Fan, Huaibo Huang, Mingrui Chen, Hongmin Liu, and Ran He. RMT: retentive networks meet vision transformers. In *Proc. IEEE Conference on Computer Vision and Pattern Recognition (CVPR)*, pages 5641–5651, 2024.
- Qihang Fan, Huaibo Huang, Yuang Ai, and Ran He. Rectifying magnitude neglect in linear attention. *CoRR*, abs/2507.00698, 2025a.
- Qihang Fan, Huaibo Huang, and Ran He. Breaking the low-rank dilemma of linear attention. In *Proc. IEEE Conference on Computer Vision and Pattern Recognition (CVPR)*, pages 25271–25280, 2025b.
- Laura Grigori and Edouard Timsit. Randomized householder QR. *CoRR*, abs/2405.10923, 2024.
- Jianyuan Guo, Kai Han, Han Wu, Yehui Tang, Xinghao Chen, Yunhe Wang, and Chang Xu. CMT: convolutional neural networks meet vision transformers. In *Proc. IEEE Conference on Computer Vision and Pattern Recognition (CVPR)*, pages 12165–12175, 2022a.
- Meng-Hao Guo, Cheng-Ze Lu, Qibin Hou, Zhengning Liu, Ming-Ming Cheng, and Shi-Min Hu. Segnext: Rethinking convolutional attention design for semantic segmentation. In *Proc. Annual Conference on Neural Information Processing (NeurIPS)*, 2022b.
- Meng-Hao Guo, Chengze Lu, Zheng-Ning Liu, Ming-Ming Cheng, and Shimin Hu. Visual attention network. *CoRR*, abs/2202.09741, 2022c.

- Dongchen Han, Xuran Pan, Yizeng Han, Shiji Song, and Gao Huang. Flatten transformer: Vision transformer using focused linear attention. In *Proc. International Conference on Computer Vision (ICCV)*, pages 5938–5948, 2023.
- Dongchen Han, Yifan Pu, Zhuofan Xia, Yizeng Han, Xuran Pan, Xiu Li, Jiwen Lu, Shiji Song, and Gao Huang. Bridging the divide: Reconsidering softmax and linear attention. In *Proc. Annual Conference on Neural Information Processing (NeurIPS)*, 2024a.
- Dongchen Han, Ziyi Wang, Zhuofan Xia, Yizeng Han, Yifan Pu, Chunjiang Ge, Jun Song, Shiji Song, Bo Zheng, and Gao Huang. Demystify mamba in vision: A linear attention perspective. In *Proc. Annual Conference on Neural Information Processing (NeurIPS)*, 2024b.
- Dongchen Han, Tianzhu Ye, Yizeng Han, ZuoFan Xia, Siyuan Pan, Pengfei Wan, Shiji Song, and Gao Huang. Agent attention: On the integration of softmax and linear attention. In *Proc. European Conference on Computer Vision (ECCV)*, pages 124–140, 2024c.
- Ali Hatamizadeh, Hongxu Yin, Greg Heinrich, Jan Kautz, and Pavlo Molchanov. Global context vision transformers. In *Proc. International Conference on Machine Learning (ICML)*, pages 12633–12646, 2023.
- Kaiming He, Georgia Gkioxari, Piotr Dollár, and Ross B. Girshick. Mask R-CNN. In *Proc. International Conference on Computer Vision (ICCV)*, pages 2980–2988, 2017.
- Qibin Hou, Cheng-Ze Lu, Ming-Ming Cheng, and Jiashi Feng. Conv2former: A simple transformer-style convnet for visual recognition. *Transactions on Pattern Analysis and Machine Intelligence*, 46(12):8274–8283, 2024.
- Tao Huang, Xiaohuan Pei, Shan You, Fei Wang, Chen Qian, and Chang Xu. Localmamba: Visual state space model with windowed selective scan. In *Proc. European Conference on Computer Vision Workshop (ECCV Workshop)*, pages 12–22, 2024.
- Angelos Katharopoulos, Apoorv Vyas, Nikolaos Pappas, and François Fleuret. Transformers are rnns: Fast autoregressive transformers with linear attention. In *Proc. International Conference on Machine Learning (ICML)*, pages 5156–5165, 2020.
- Manjin Kim, Paul Hongsuck Seo, Cordelia Schmid, and Minsu Cho. Learning correlation structures for vision transformers. In *Proc. IEEE Conference on Computer Vision and Pattern Recognition (CVPR)*, pages 18941–18951, 2024.
- Youngwan Lee, Jonghee Kim, Jeffrey Willette, and Sung Ju Hwang. Mpvit: Multi-path vision transformer for dense prediction. In *Proc. IEEE Conference on Computer Vision and Pattern Recognition (CVPR)*, pages 7277–7286, 2022.
- Siyuan Li, Zedong Wang, Zicheng Liu, Cheng Tan, Haitao Lin, Di Wu, Zhiyuan Chen, Jiangbin Zheng, and Stan Z. Li. Moganet: Multi-order gated aggregation network. In *Proc. International Conference on Learning Representations (ICLR)*, 2024.
- Jingyun Liang, Jie Zhang Cao, Guolei Sun, Kai Zhang, Luc Van Gool, and Radu Timofte. Swinir: Image restoration using swin transformer. In *Proc. International Conference on Computer Vision (ICCV)*, pages 1833–1844, 2021.
- Bencheng Liao, Xinggang Wang, Lianghui Zhu, Qian Zhang, and Chang Huang. Vig: Linear-complexity visual sequence learning with gated linear attention. In *Proc. Association for the Advancement of Artificial Intelligence (AAAI)*, pages 5182–5190, 2025.
- Tsung-Yi Lin, Michael Maire, Serge J. Belongie, James Hays, Pietro Perona, Deva Ramanan, Piotr Dollár, and C. Lawrence Zitnick. Microsoft COCO: common objects in context. In *Proc. European Conference on Computer Vision (ECCV)*, pages 740–755, 2014.
- Tsung-Yi Lin, Priya Goyal, Ross B. Girshick, Kaiming He, and Piotr Dollár. Focal loss for dense object detection. In *Proc. International Conference on Computer Vision (ICCV)*, pages 2999–3007, 2017.
- Weifeng Lin, Ziheng Wu, Jiayu Chen, Jun Huang, and Lianwen Jin. Scale-aware modulation meet transformer. In *Proc. International Conference on Learning Representations (ICLR)*, pages 5992–6003, 2023.
- Yue Liu, Yunjie Tian, Yuzhong Zhao, Hongtian Yu, Lingxi Xie, Yaowei Wang, Qixiang Ye, Jianbin Jiao, and Yunfan Liu. Vmamba: Visual state space model. In *Proc. Annual Conference on Neural Information Processing (NeurIPS)*, 2024.

Ze Liu, Yutong Lin, Yue Cao, Han Hu, Yixuan Wei, Zheng Zhang, Stephen Lin, and Baining Guo. Swin transformer: Hierarchical vision transformer using shifted windows. In *Proc. International Conference on Computer Vision (ICCV)*, pages 9992–10002, 2021.

Ze Liu, Han Hu, Yutong Lin, Zhuliang Yao, Zhenda Xie, Yixuan Wei, Jia Ning, Yue Cao, Zheng Zhang, Li Dong, Furu Wei, and Baining Guo. Swin transformer V2: scaling up capacity and resolution. In *Proc. IEEE Conference on Computer Vision and Pattern Recognition (CVPR)*, pages 11999–12009, 2022.

Jiachen Lu, Junge Zhang, Xiatian Zhu, Jianfeng Feng, Tao Xiang, and Li Zhang. Softmax-free linear transformers. *International Journal of Computer Vision*, 132:3355–3374, 2024.

Nanye Ma, Mark Goldstein, Michael S. Albergo, Nicholas M. Boffi, Eric Vanden-Eijnden, and Saining Xie. Sit: Exploring flow and diffusion-based generative models with scalable interpolant transformers. In *Proc. European Conference on Computer Vision (ECCV)*, 2024.

Weikang Meng, Yadan Luo, Xin Li, Dongmei Jiang, and Zheng Zhang. Polaformer: Polarity-aware linear attention for vision transformers. In *Proc. International Conference on Learning Representations (ICLR)*, 2025.

Zakaria Mhammedi, Andrew Hellicar, Ashfaqur Rahman, and James Bailey. Efficient orthogonal parametrisation of recurrent neural networks using householder reflections. In *International Conference on Machine Learning*, pages 2401–2409. PMLR, 2017.

MiniMax, Aonian Li, Bangwei Gong, and et al. Minimax-01: Scaling foundation models with lightning attention. *CoRR*, abs/2501.08313, 2025.

Yury Nahshan, Joseph Kampeas, and Emir Haleva. Linear log-normal attention with unbiased concentration. In *Proc. International Conference on Learning Representations (ICLR)*, 2024.

William Peebles and Saining Xie. Scalable diffusion models with transformers. In *Proc. International Conference on Computer Vision (ICCV)*, pages 4172–4182, 2023.

Yifan Pu, Zhuofan Xia, Jiayi Guo, Dongchen Han, Qixiu Li, Duo Li, Yuhui Yuan, Ji Li, Yizeng Han, Shiji Song, Gao Huang, and Xiu Li. Efficient diffusion transformer with step-wise dynamic attention mediators. In *Proc. European Conference on Computer Vision (ECCV)*, 2024.

Zhen Qin, Weixuan Sun, Hui Deng, Dongxu Li, Yunshen Wei, Baohong Lv, Junjie Yan, Lingpeng Kong, and Yiran Zhong. Cosformer: Rethinking softmax in attention. In *Proc. International Conference on Learning Representations (ICLR)*, 2022.

Zhen Qin, Weigao Sun, Dong Li, Xuyang Shen, Weixuan Sun, and Yiran Zhong. Various lengths, constant speed: Efficient language modeling with lightning attention. In *Proc. International Conference on Machine Learning (ICML)*, 2024.

Zhuoran Shen, Mingyuan Zhang, Haiyu Zhao, Shuai Yi, and Hongsheng Li. Efficient attention: Attention with linear complexities. In *Proc. Winter Conference on Applications of Computer Vision (WACV)*, pages 3530–3538, 2021.

Hugo Touvron, Matthieu Cord, Matthijs Douze, Francisco Massa, Alexandre Sablayrolles, and Hervé Jégou. Training data-efficient image transformers & distillation through attention. In *Proc. International Conference on Machine Learning (ICML)*, pages 10347–10357, 2021.

Zhengzhong Tu, Hossein Talebi, Han Zhang, Feng Yang, Peyman Milanfar, Alan C. Bovik, and Yinxiao Li. Maxvit: Multi-axis vision transformer. In *Proc. European Conference on Computer Vision (ECCV)*, pages 459–479, 2022.

Ashish Vaswani, Noam Shazeer, Niki Parmar, Jakob Uszkoreit, Llion Jones, Aidan N. Gomez, Łukasz Kaiser, and Illia Polosukhin. Attention is all you need. In *Proc. Annual Conference on Neural Information Processing (NeurIPS)*, pages 5998–6008, 2017.

Madhusudan Verma. Revisiting linformer with a modified self-attention with linear complexity. *CoRR*, abs/2101.10277, 2021.

Dustin Wang, Rui-Jie Zhu, Steven Abreu, Yong Shan, Taylor Kergan, Yuqi Pan, Yuhong Chou, Zheng Li, Ge Zhang, Wenhao Huang, and Jason Eshraghian. A systematic analysis of hybrid linear attention. *CoRR*, abs/2507.06457, 2025.

Wenhai Wang, Enze Xie, Xiang Li, Deng-Ping Fan, Kaitao Song, Ding Liang, Tong Lu, Ping Luo, and Ling Shao. Pyramid vision transformer: A versatile backbone for dense prediction without convolutions. In *Proc. International Conference on Computer Vision (ICCV)*, pages 548–558, 2021.

Wenhai Wang, Enze Xie, Xiang Li, Deng Ping Fan, Kaitao Song, Ding Liang, Tong Lu, Ping Luo, and Ling Shao. Pvt v2: Improved baselines with pyramid vision transformer. *Computational Visual Media*, 8:415–424, 2022.

Wenhai Wang, Jifeng Dai, Zhe Chen, Zhenhang Huang, Zhiqi Li, Xizhou Zhu, Xiaowei Hu, Tong Lu, Lewei Lu, Hongsheng Li, Xiaogang Wang, and Yu Qiao. Internimage: Exploring large-scale vision foundation models with deformable convolutions. In *Proc. IEEE Conference on Computer Vision and Pattern Recognition (CVPR)*, pages 14408–14419, 2023.

Zhaozhi Wang, Yue Liu, Yunfan Liu, Hongtian Yu, Yaowei Wang, Qixiang Ye, and Yunjie Tian. vheat: Building vision models upon heat conduction. *CoRR*, abs/2405.16555, 2024.

Enze Xie, Wenhai Wang, Zhiding Yu, Anima Anandkumar, José M. Álvarez, and Ping Luo. Segformer: Simple and efficient design for semantic segmentation with transformers. In *Proc. Annual Conference on Neural Information Processing (NeurIPS)*, pages 12077–12090, 2021.

Haotian Yan, Ming Wu, and Chuang Zhang. Multi-scale representations by varying window attention for semantic segmentation. In *The Twelfth International Conference on Learning Representations, ICLR 2024, Vienna, Austria, May 7-11, 2024*, 2024.

Chenglin Yang, Siyuan Qiao, Qihang Yu, Xiaoding Yuan, Yukun Zhu, Alan L. Yuille, Hartwig Adam, and Liang-Chieh Chen. MOAT: alternating mobile convolution and attention brings strong vision models. In *Proc. International Conference on Learning Representations (ICLR)*, 2023.

Haoran You, Yunyang Xiong, Xiaoliang Dai, Bichen Wu, Peizhao Zhang, Haoqi Fan, Peter Vajda, and Yingyan Celine Lin. Castling-vit: Compressing self-attention via switching towards linear-angular attention at vision transformer inference. In *Proc. IEEE Conference on Computer Vision and Pattern Recognition (CVPR)*, pages 14431–14442, 2023.

Weihao Yu and Xinchao Wang. Mambaout: Do we really need mamba for vision? In *Proc. IEEE Conference on Computer Vision and Pattern Recognition (CVPR)*, pages 4484–4496, 2025.

Kun Zeng, Hanjiang Lin, Zhiqiang Yan, and Jinsheng Fang. Densely connected transformer with linear self-attention for lightweight image super-resolution. *IEEE Trans. Instrum. Meas.*, 72:1–12, 2023.

Michael Zhang, Kush Bhatia, Hermann Kumbong, and Christopher Ré. The hedgehog & the porcupine: Expressive linear attentions with softmax mimicry. In *Proc. International Conference on Learning Representations (ICLR)*, 2024.

Bolei Zhou, Hang Zhao, Xavier Puig, Tete Xiao, Sanja Fidler, Adela Barriuso, and Antonio Torralba. Semantic understanding of scenes through the ADE20K dataset. *International Journal of Computer Vision*, 127:302–321, 2019.

Zhanchao Zhou, Xiaodong Chen, Haoxing Chen, Zhenzhong Lan, and Jianguo Li. Knocking-heads attention. *CoRR*, abs/2510.23052, 2025.

Lianghui Zhu, Bencheng Liao, Qian Zhang, Xinlong Wang, Wenyu Liu, and Xinggang Wang. Vision mamba: Efficient visual representation learning with bidirectional state space model. In *Proc. International Conference on Machine Learning (ICML)*, 2024.

Lianghui Zhu, Zilong Huang, Bencheng Liao, Jun Hao Liew, Hanshu Yan, Jiashi Feng, and Xinggang Wang. Dig: Scalable and efficient diffusion models with gated linear attention. In *Proc. IEEE Conference on Computer Vision and Pattern Recognition (CVPR)*, pages 7664–7674, 2025.

A Appendix

- [A.1 Model Settings](#).
- [A.2 Ablation Study](#).
- [A.3 Visualizations](#).
- [A.4 Discussion](#). Efficient Implement Discussion.

A.1 Model Settings

Consistent with established works (Fan et al., 2025b, 2024; Liu et al., 2021), we develope a set of Mirror-LA backbones by only replace the non-negative activations with our reflecting feature map, each with varying configurations of block count and channel dimensions across their respective stages whose the ratio of MLP is set to 3.5. The architecture details are illustrated in the Tab. 6.

Table 6 Architecture setting details of MirrorLA.

MODEL	PARAM	FLOPS	BLOCKS	CHANNELS	HEADS
MirrorLA-XT	6M	0.6G	[2, 2, 2, 2]	[32, 64, 128, 384]	[1, 2, 4, 8]
MirrorLA-T	15M	2.6G	[2, 2, 6, 2]	[64, 128, 256, 512]	[1, 2, 4, 8]
MirrorLA-S	26M	4.9G	[3, 5, 9, 3]	[64, 128, 320, 512]	[1, 2, 5, 8]
MirrorLA-B	48M	10.6G	[4, 6, 12, 6]	[96, 192, 384, 512]	[1, 2, 6, 8]
MirrorLA-L	95M	17.3G	[4, 7, 19, 8]	[96, 192, 448, 640]	[1, 2, 7, 10]

A.2 Ablation Study

Comparison with Other Linear Attention. To ensure a rigorous and fair comparison, we adhere to the evaluation protocol established by FLatten-Transformer using the Swin-T architecture. MirrorLA is designed as a modular enhancement: we simply insert our reflecting feature map operation immediately before the non-negativity constraint, while keeping all other components—including specific "spiky" activation functions—entirely unchanged. Results are shown in Tab. 7

Table 7 Comparison with other linear attention models on the Swin-T setting.

METHOD	PARAMS	FLOPS	ACC. (%)
Swin-T (Liu et al., 2021)	28M	4.4G	81.2
Hydra Attn (Bolya et al., 2022)	29M	4.5G	80.7
Efficient Attn (Shen et al., 2021)	29M	4.5G	81.0
Linear Angular (You et al., 2023)	29M	4.5G	79.4
FLatten Attn (Han et al., 2023)	29M	4.5G	82.1
Agent Attn (Han et al., 2024c)	29M	4.5G	82.6
InLine Attn (Han et al., 2024a)	30M	4.5G	82.4
PolaFormer (Meng et al., 2025)	29M	4.5G	82.6
ReLU+LA	28M	4.6G	81.8
ReLU+MirrorLA	28M	4.6G	82.4

Hyperparameters and components Ablations. We study the impact of key design choices in MirrorLA on the XT setting. Specifically, we vary the λ used in sigmoid $\left(\frac{\lambda}{\sigma_m^2 + \varepsilon}\right)$, the maximum angular perturbation α_{\max} , and whether to enable the full variant and the cross-head reflection. As shown in Tab. 8, the default setting achieves the best accuracy. Disabling the full variant causes a 0.5 drop, while removing cross-head reflection reduces accuracy by 0.3.

Table 8 Hyperparameter ablations for MirrorLA.

λ	α_{\max}	FULL	HEAD	Acc. (%)
1	$\pi/2$	✓	✓	76.0
1	$\pi/2$		✓	75.5-0.5
1	$\pi/2$	✓		75.7-0.3
0.5	$\pi/2$	✓	✓	75.7-0.3
0.25	$\pi/2$	✓	✓	75.8-0.2
1	$\pi/4$	✓	✓	75.9-0.1
1	$\pi/8$	✓	✓	75.8-0.2

More Results. We additionally conduct semantic segmentation experiments using the MMSegmentation framework (Contributors, 2018). Following the same settings as PVT (Wang et al., 2021), we train models with a Semantic FPN decoder. Under the same model scale, MirrorLA achieves the best performance.

Table 9 More semantic segmentation results. Results on Semantic FPN 80K.

METHOD	PARA	FLOPs	MIoU
VAN-B1 (Guo et al., 2022c)	18M	140G	42.9
PVT-v2-B1 Wang et al. (2022)	18M	136G	42.5
RMT-T (Fan et al., 2024)	17M	136G	46.4
FL-PVT-T (Han et al., 2023)	16M	169G	37.2
Agent-PVT-T (Han et al., 2024c)	15M	147G	40.2
RAVLT-T (Fan et al., 2025b)	18M	136G	47.5
MirrorLA-T	18M	136G	47.7

A.3 Visualizations

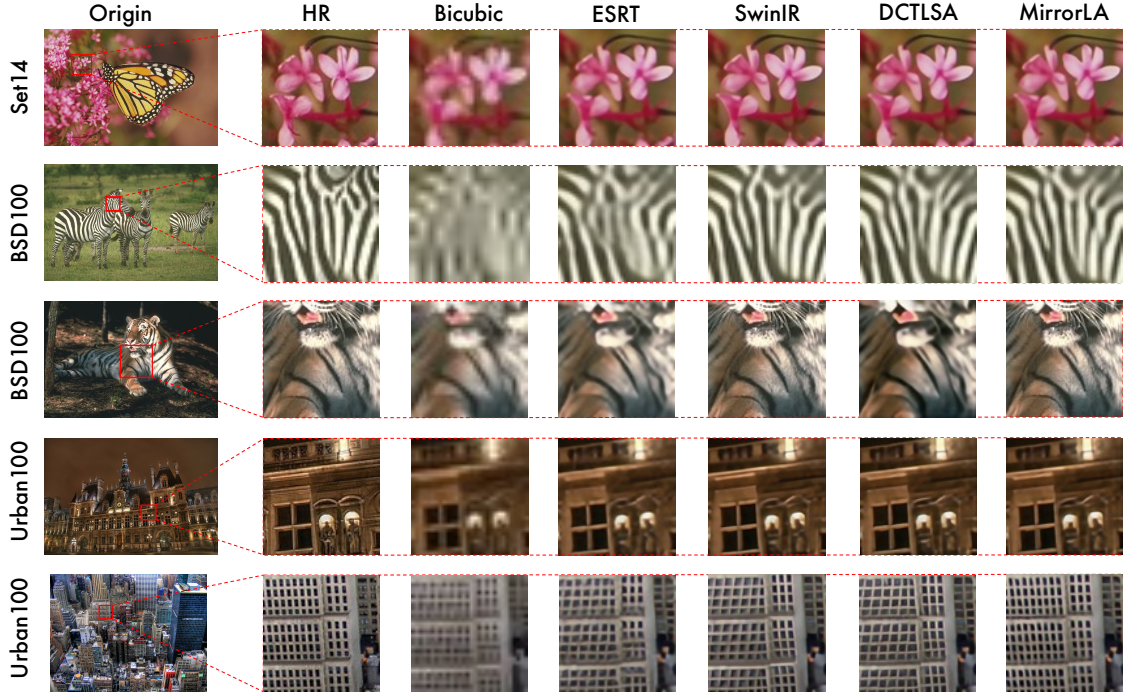


Figure 4 More visualizations on super-resolution tasks. Our model produces more clear boundaries, more accurate shapes, and finer-grained textures compared to baselines.

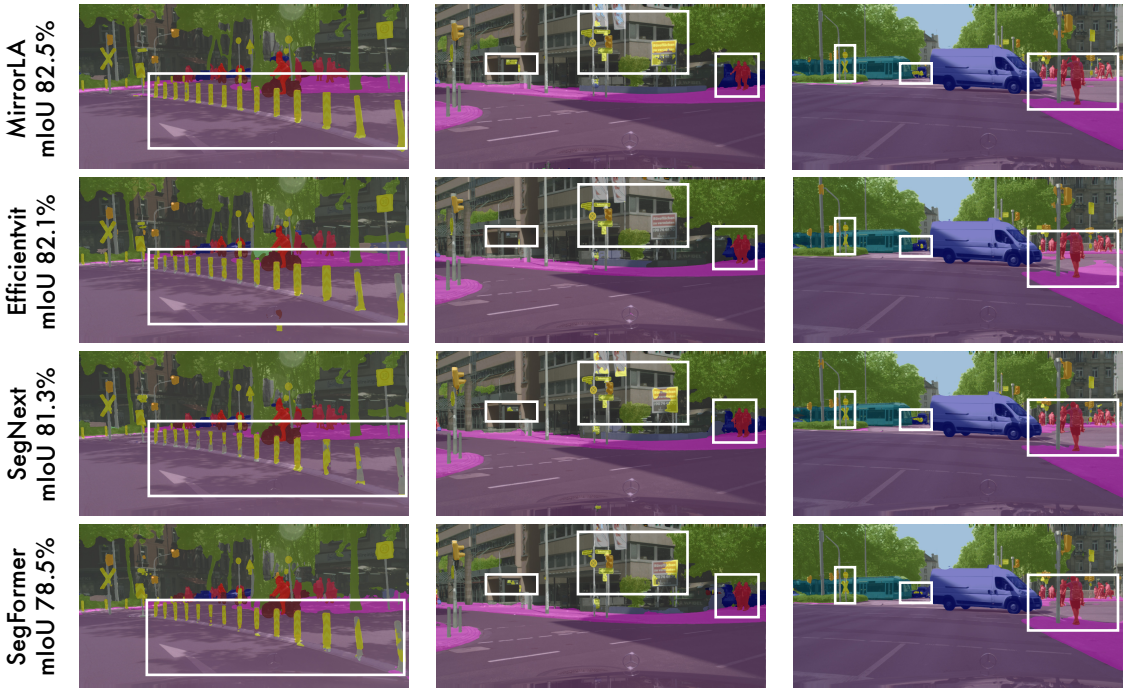


Figure 5 Visualization results on semantic segmentation. Compared to other methods, our approach more accurately delineates different objects, effectively avoiding missing predictions and boundary ambiguities.

A.4 Discussion

Future Work: Hardware-Aware Design. The practical utility of linear attention models increasingly relies on high-performance acceleration libraries. A prominent example is Flash Linear Attention (FLA), a specialized Triton-based library designed for the efficient computation of linear attention. While MirrorLA demonstrates superior representational capacity, its full integration with such high-performance hardware kernels presents an intriguing avenue for future research. Currently, the implementation of our geometric modulations, such as Householder reflections, is primarily optimized at the functional level.

In future work, we aim to implement block-wise architectural optimizations to better align with the parallel processing logic of modern GPUs. Specifically, we plan to develop dedicated Triton-based kernels to fuse these geometric operations directly into the FLA framework. Such hardware-aware synergy would be particularly beneficial for high-dimensional 2D vision tasks, where custom tiling strategies could mitigate register pressure and SRAM constraints. By bridging the gap between active geometric modeling and low-level operator fusion, we believe MirrorLA can achieve a more optimal balance between theoretical expressivity and practical inference throughput across diverse modalities.